Available online at www.sciencedirect.com
ScienceDirect
Journal of Power Sources 162 (2006) 132–140
JOURNAL OF POWER SOURCES
www.elsevier.com/locate/jpowsour

Effects of annealing treatment and pH on preparation of citrate-stabilized PtRu/C catalyst

Yuqin Xu [a], Xiaofeng Xie [a,*], Jianwei Guo [a], Shubo Wang [a], Yaowu Wang [a], V.K. Mathur [b]

[a] *Institute of Nuclear and New Energy Technology, Tsinghua University, Beijing 100084, China*
[b] *Department of Chemical Engineering, University of New Hampshire, NH 03824, United States*

Received 17 June 2006; received in revised form 9 July 2006; accepted 10 July 2006
Available online 22 August 2006

Abstract

The annealing treatment and pH were controlled to prepare a bimetallic PtRu/C anode catalyst by the citrate-stabilized chemical reduction method. X-ray diffraction and X-ray photoelectron spectra revealed that the catalyst before the annealing treatment showed smaller size particles mainly composed of metallic platinum and hydrous ruthenium oxide. The anhydrous RuO_2 increased with increase in the annealing temperature from 250 °C to 400 °C. The linear sweep voltammetry (LSV) results showed that the non-annealed catalyst had the highest current density at a given potential. Also, the particle size varied with the stabilizing pH. A homogenous catalyst was prepared at a pH of 7 in the laboratory. The particle size was about 2.39 ± 0.46 nm with 14.62 at% ruthenium in the PtRu alloy. The maximum LSV current density was 66.4 mA mg^{-1} PtRu at 0.45 V with an onset potential of 0.12 V (versus SCE). The catalyst when tested in a single cell DMFC produced a power density of 67.5 mW cm^{-2} at a current density of 240 mA cm^{-2}.

Keywords: Direct methanol fuel cell; PtRu/C; Citrate; Annealing treatment; pH

1. Introduction

An investigation of methanol eletrooxidation in a direct methanol fuel cell (DMFC) shows a severe poisoning of a conventional Pt/C catalyst because of the formation of by-products such as CO. However, a bimetallic PtRu/C catalyst can perform better due to electronic effects [1,2] and the bi-functional mechanism [3,4] in which the active oxygen required for the methanol eletrooxidation can be provided by ruthenium dissociating H_2O at a lower positive potential than metallic platinum. Recently, much attention has been directed to the study of the relationship between the cell performance and the microstructure of catalysts. It has been suggested that the PtRu alloy structure contributes little to the performance of the catalysts [5]. It is the hydrous ruthenium oxide RuO_xH_y (or $RuO_2{\cdot}xH_2O$) and not the PtRu alloy or the anhydrous RuO_2, that improves the performance of an electrocatalyst [6,7]. This conclusion has been supported by Lu et al. [8] through a pattern-recognition methodology. Thus, the development of ruthenium oxide supported platinum catalysts, through the design and selectivity of the morphology, has become the subject of several investigations [9].

The performance of bimetallic PtRu/C catalysts is dependent on a specific process [10], size, surface structure [11], morphology, etc. Since Turkevich used citrate for the preparation of Pt nanoparticles in 1986 [12], several researches are studying the use of citrate as a water-soluble stabilizer to obtain Pt nanoparticles. Lin et al. [13] experimentally demonstrated the different roles of citrate as a reductant or a stabilizer and that the reducing reaction could not take place below 90 °C. The size-dependence of the Pt/C catalysts on the concentration of citric acid has been reported by Guo et al. [14] who had proposed a citrate complexation stabilizing mechanism. The electrochemical removal of citrate stabilizer and the immobilization of Pt hydrosol are proposed in another work [15]. The commonly used annealing treatment decreases the electrochemical activity of the catalyst [16]. Unfortunately, not many studies have been reported in this area. On the other hand, it has been known for sometime that pH influences the chemical equilibrium of weak carbonyl acid and thus the stabilizing effect [17]. Turkevich et al. [12] has studied pH effects on Pt nanoparticles prepared with citrate as a

* Corresponding author. Tel.: +86 10 62784827; fax: +86 10 62881150.
E-mail address: xiexf@tsinghua.edu.cn (X. Xie).

0378-7753/$ – see front matter © 2006 Published by Elsevier B.V.
doi:10.1016/j.jpowsour.2006.07.021

reductant and a stabilizer. Recently, Shimazaki et al. [16] have discussed the malfunction of citric acid as a stabilizer in acid condition.

In the present study, citrate-stabilized PtRu/C anode catalysts were prepared systematically. Annealing treatment and stabilizing pH were separately controlled to develop homogeneous dispersed catalyst with adequate hydrous ruthenium oxide to promote the catalyst activity. X-ray diffraction (XRD), X-ray photoelectron spectrum (XPS), transmission electron microscopy (TEM) and the electrochemical LSV were carried out to measure the catalyst compositions, alloying, size and size distribution. Further, a single cell DMFC performance measurement was made to demonstrate the electrocatalytic activities of a prepared catalyst.

2. Experimental procedures

2.1. Preparation of PtRu/C electrocatalysts

A 20 wt.% PtRu/C electrocatalyst with a Pt to Ru molar ratio of 1:1 was prepared by citrate-stabilized chemical reduction method. Vulcan carbon powder XC-72R with a specific BET area of 250 $m^2\ g^{-1}$ and an average size of 40 nm was purchased from Cabot Corporation and used as a support. 114 mg of XC-72R which was pretreated for 2 h at 600 °C in nitrogen atmosphere was dispersed in deionized water. Then, 5 ml of 9.65 mM chloroplatinic acid and 6 ml of 7.65 mM ruthenium chloride solutions were added. Sodium citrate was added in a molar ratio of 2:1 to platinum. The suspension was diluted to 100 ml and ultrasonicated for 30 min. Subsequently, a 1 M NaOH aqueous solution was added drop wise to adjust the pH to 11, followed by vigorous stirring at 50 °C for 10 h to achieve an equilibrium. An excess of 1 M sodium borohydride solution was added to the ink to serve as a reducing agent. The temperature was maintained at 50 °C for another 4 h to ensure a complete reduction. All chemicals used were analytical grade. The prepared catalysts were filtered, washed thoroughly and dried in an air oven at 80 °C for 2 h. The annealing treatments were conducted at 250 °C and 400 °C for 2 h in a tube furnace under nitrogen atmosphere. Four other such catalysts were prepared at the pH values of 5, 7, 9 and 13 to study pH effect on the electrocatalytic activity of PtRu/C catalysts.

2.2. Physicochemical characterizations

Powder X-ray diffraction patterns were obtained using a Bruker D8-Discover micro X-ray diffractometer with a Cu Kα X radiation source ($\lambda_{Cu\ K\alpha}$ = 1.5406 Å) at 40 kV and 40 mA. The particle dispersion, size and size distribution of the electrocatalysts were characterized by TEM techniques using the JEOL-200CX instrument operating at 200 kV. High-resolution TEM patterns of nanocrystals were studied on a JEM-2010F microscope at 200 kV. Further, the energy dispersive spectroscopy (EDS) analysis was carried out with an Oxford INCA-IET200 attached to the microscope. The TEM sample is prepared by ultrasonically suspending the catalyst in ethanol and then depositing a small drop of the suspension onto a Ø 3 mm copper grid covered with continuous amorphous carbon film. The X-ray photoelectron spectrum (XPS) was obtained with a PHI Quantera SXM spectrometer using Al monochromatic X-ray source operating at 4.0 kV. Observed spectra were deconvoluted by the Peakfit software fitted with the Gaussian function.

2.3. Electrochemical measurements

Electrochemical measurements were carried out by a standard three electrode cell at ambient temperature with a saturated calomel electrode (SCE) as the reference electrode, Pt foil as the counter electrode, and a glassy carbon (GC) electrode with the synthesized catalyst as the working electrode. All potentials reported in this paper are with SCE as the reference electrode. The GC electrode, with a diameter of 3 mm, was polished with a 0.05 μm alumina suspension before each measurement. The preparation of the test electrode was as follows: 5 mg catalyst was dispersed into the mixture of 1.65 ml ethanol and 0.35 ml 0.1 wt.% Nafion solution by sonicating for 20 min, and then 20 μl of the slurry was pipetted with a syringe and spread onto the mirror-polished GC electrode to obtain a metal loading of 0.01 mg PtRu. After totally covered, the working GC electrode was dried for 10 min at 65 °C. The three electrode cell system was purged with nitrogen gas for 30 min before the electrochemical analysis. All electrochemical measurements were made under nitrogen atmosphere. The linear sweep voltammetry was performed with a potentiostat (EG&G Princeton, Model 263A) in the range from −0.25 to 0.45 V after proper activation in 0.5 M H_2SO_4 solution. The third LSV curve was recorded at 5 mV s^{-1} in the solution of 0.5 M H_2SO_4 and 0.5 M CH_3OH.

2.4. Membrane electrode assembly (MEA) fabrication and fuel cell testing

The above prepared catalyst was tested as a methanol electrooxidation catalyst in a single direct methanol fuel cell. Catalyst was coated on either side of the membrane using the catalyst coated membrane (CCM) technique. Nafion 115 membrane was used as the membrane material. A mixture of catalyst and 5 wt.% Nafion solution was first ultrasonicated and then uniformly sprayed onto the membrane with a cross-section area of 5 cm^2 and dried, followed by hot pressing at 150 °C and 5 MPa for 2 min with the gas diffusion layers(GDLs). The gas diffusion layers used in the MEA were prepared from hydrophobic carbon paper Toray-90, coated with a mixture of PTFE and XC-72R powder. The anode catalyst has a loading of 2.73 mg PtRu cm^{-2}. The cathode catalyst was 60 wt.% Pt/C catalyst (Johnson Matthey) with a loading of 3 mg Pt cm^{-2}.

The performance test was conducted in a single cell DMFC at 60 °C and 75 °C after being activated. The anode fuel was 1 M methanol aqueous solution at a flow rate of 3 mL min^{-1}. The cathode uses air at a flow rate of 300 standard cubic centimeters per minute (sccm) at zero psig.

3. Results and discussion

3.1. Effects of annealing temperature

The XRD pattern of the prepared catalyst was presented in Fig. 1a. The XRD results of the same sample after 250 °C and 400 °C annealing treatment are shown as curves b and c, respectively. There are four peaks of metal Pt face-centered cubic (fcc) diffraction—Pt(1 1 1), Pt(2 0 0), Pt(2 2 0) and Pt(3 1 1) and are a little shifted to a higher 2θ values from 39.76°, 46.24°, 67.45° and 81.28° for pure Pt fcc indicating the reduction in lattice constants because of Ru substitution. The lattice parameters, for example, for PtRu alloy in Pt(2 2 0) can be estimated from XRD diffractions by Vegard's law [18].

$$a_{\mathrm{fcc}} = \frac{\sqrt{2}\lambda_{\mathrm{Cu\,K}\alpha}}{\sin\theta_{\max}} \quad (1)$$

where $\lambda_{\mathrm{Cu\,K}\alpha} = 1.5406$ Å for the X-ray wavelength. $\theta_{\max}$ was the angle at the maximum Pt(2 2 0) peak. Also, the alloying Ru atomic fraction x_{Ru} could be estimated from the following relationship [19].

$$x_{\mathrm{Ru}} = \frac{a_{\mathrm{fcc0}} - a_{\mathrm{fcc}}}{\mathrm{Ku}} \quad (2)$$

where lattice constant $a_{\mathrm{fcc0}} = 3.9155$ Å for supported platinum obtained from XRD data. Ku = 0.124 Å is a constant factor. The calculated results were 34.8%, 30.8% and 36.4% for the catalysts before and after annealed at 250 °C and 400 °C, respectively, showing that the annealing treatment did not significantly affect the degree of alloying. Meanwhile, no recognizable metallic ruthenium diffraction was observed in Fig. 1a, implying that the ruthenium may not only enter Pt fcc-lattice to establish PtRu alloy but partially exist as hydrous ruthenium oxide, not being clearly discerned by X-ray diffraction [7]. Furthermore, new diffraction peaks at the 2θ positions of 28.1°, 35.1° and 54.3° typically indicate the presence of anhydrous ruthenium oxides rather than the platinum oxides which could not be formed by annealing below 400 °C [6]. A conclusion might be drawn that the hydrous $RuO_2{\cdot}xH_2O$ tends to become anhydrous RuO_2 by self-dehydration. After annealed at 400 °C, the catalyst XRD curve has noticeable RuO_2 diffraction peaks. Even at 250 °C, a proposal temperature for the removal of citrate [16], this diffraction occurs. The particles grow in size as the annealing temperature increases as shown by XRD patterns, the peaks becoming narrow and pointed. According to Scherrer equation [18], the catalyst has the smallest size of 2.84 nm before annealing and the size increase to 3.66 nm, and 4.76 nm after annealed at 250 °C and 400 °C, respectively.

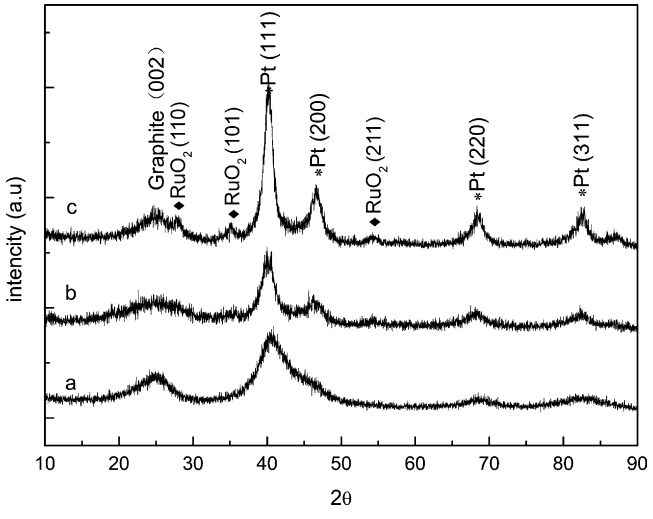

Fig. 1. XRD patterns of PtRu/C catalysts before annealing (a), after annealing at 250 °C (b) and 400 °C (c).

The XPS spectra of the catalysts before and after annealing treatment at 400 °C are shown in Fig. 2. The results obtained by the deconvolution of the XPS spectra are summarized in Table 1. The Pt4f spectrum consists of three couples of doublets with low binding energies (BE) of 71.29 eV, 72.6 eV, and 74.63 eV. The most intense doublet of 71.29 eV and 74.63 eV are attributed to a zero-valence metallic platinum which is shifted a little to a higher BE than that of the bulk Pt element (71.29 eV and 74.63 eV) due to the interactions between Pt nanoparticles and carbon support or the ruthenium species [20]. The doublet of 72.47 eV and 75.78 eV indicates the presence of amorphous Pt(II) species, and the broad doublet of 76.4 eV and 77.96 eV is assigned to the Pt(IV) species. The percentage of metallic platinum in the catalyst surface increased from 55.15% to 62.80% after the annealing treatment probably due to some removal of the citrate stabilizer. Since the Ru3p spectra are too weak to be precisely extracted from the noise background, the Ru3d region together with C1s signal are comprehensively analyzed. In parallel, a Pt/C catalyst without Ru was prepared by the same method and the C1s XPS spectrum (not shown here) was analyzed, being deconvoluted into three peaks, 284.4 eV, 285.6 eV and 288.1 eV. The most intensive peak of 284.4 eV was assigned to carbon graphite C1s, and the other two peaks are both attributed to carbon bonded to oxygen, –C=O and COO^-, respectively [21]. As for the PtRu/C, the BE of 280.1 eV and 280.7 eV are assigned to metallic Ru and anhydrous RuO_2 (see the Fig. 2c and d). Unfortunately, the hydrous RuO_xH_y at 282.2 eV [22] and the higher oxidation state ruthenium, RuO_3 at 282.7 eV or RuO_4 at 284 eV [20] could not be accurately determined because of the overlap with C1s signal. The XPS data (Table 1) suggest that the atomic ratio of anhydrous RuO_2 to metallic Ru increased from 4:6 to nearly 9:1 after 400 °C annealing treatment, probably due to the loss of water in hydrous $RuO_2{\cdot}xH_2O$ from changing to anhydrous RuO_2 initiated below 200 °C, or a slight oxidation of metallic Ru to anhydrous RuO_2 by trace oxygen in the nitrogen as well [7]. This enrichment in anhydrous RuO_2, in conjunction with the appearance of RuO_2 diffraction peaks in XRD spectrum, would explain the discrepancy in electrochemical activity as discussed below.

Fig. 3 shows the LSV curves for methanol electrooxidation on the catalysts before and after catalyst was annealed at 250 °C and 400 °C. Each of the curves is the average of three parallel measurements. The LSV upper potential was fixed as 0.45 V to avoid anodic Ru electrooxidation and dissolution at a higher potential. The figure shows that the non-annealed catalyst has the highest current density (34.2 mA mg^{-1} PtRu) at the potential of

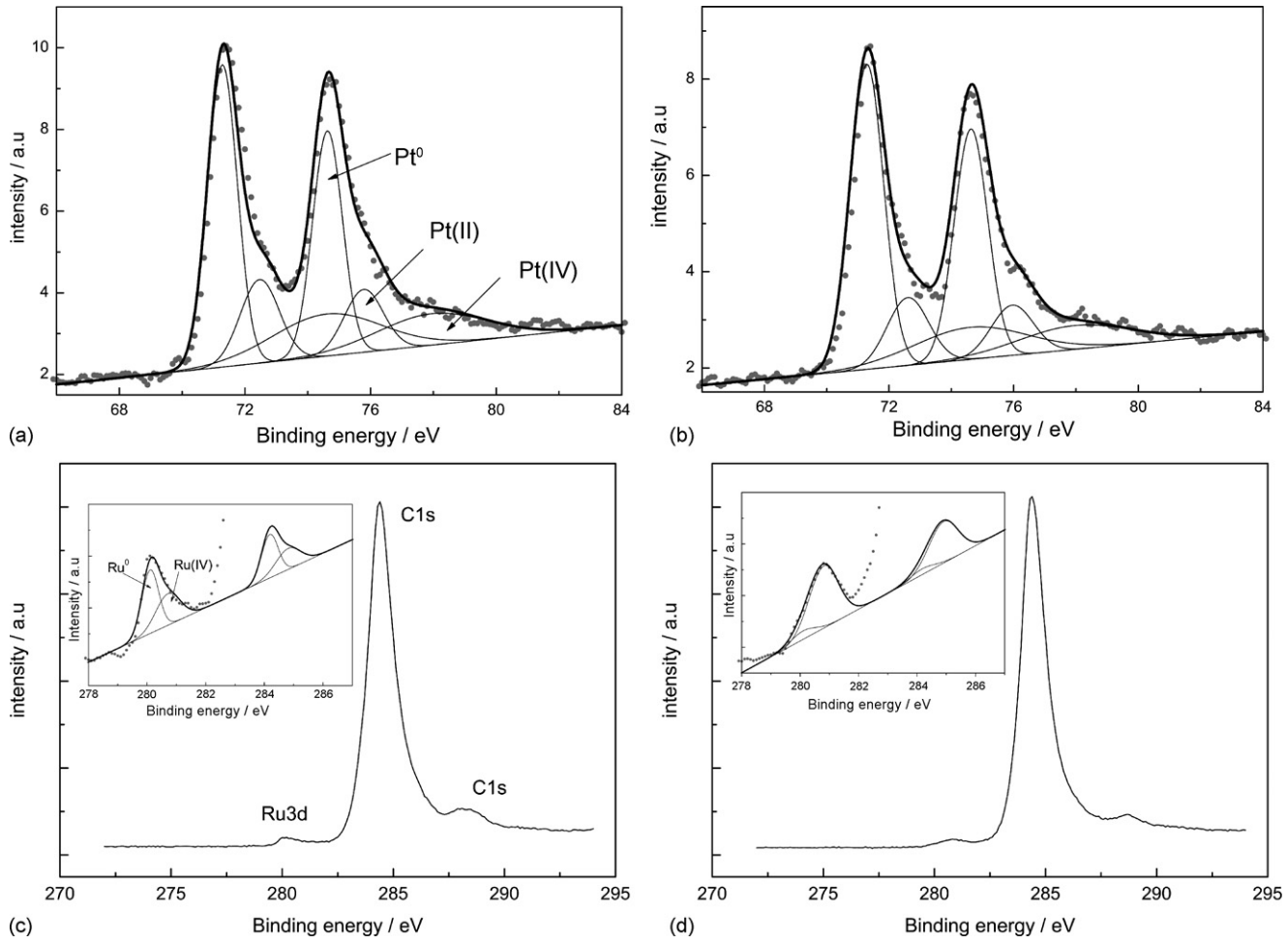

Fig. 2. Regional XPS of 20 wt.% PtRu/C nanocatalyst in Pt4f before annealing (a), after annealing at 400 °C (b); and in C1s + Ru3d before annealing (c), after annealing at 400 °C (d). The inserts in (c and d) are magnified deconvolution spectra between 278 eV and 282 eV for Ru3d.

Table 1
Binding energies and surface compositions from deconvolution of XPS spectra for catalysts before and after annealing at 400 °C

Catalyst	Species	Binding energy (eV)	Peak half width (eV)	Possible chemical state	Relative concentrations (%)
PtRu/C (before annealing)	Pt4f	71.29	1.12	Pt^0	31.61
		74.63	1.12	Pt^0	23.54
		72.47	1.46	Pt(II)	11.04
		75.78	1.45	Pt(II)	8.26
		76.40	4.06	Pt(IV)	14.57
		77.96	4.09	Pt(IV)	10.97
	Ru3d[a]	280.1	0.67	Ru^0	35.55
		284.2	0.66	Ru^0	24.11
		280.7	0.98	Ru(IV)	24.19
		284.8	0.99	Ru(IV)	16.16
PtRu/C (after annealing at 400 °C)	Pt4f	71.29	1.27	Pt^0	35.78
		74.63	1.27	Pt^0	27.02
		72.60	1.57	Pt(II)	9.61
		75.96	1.58	Pt(II)	7.19
		74.61	5.25	Pt(IV)	11.68
		77.96	4.27	Pt(IV)	8.72
	Ru3d	280.1	1.0	Ru^0	6.32
		284.2	1.0	Ru^0	4.29
		280.8	1.17	Ru(IV)	53.59
		284.9	1.18	Ru(IV)	35.80

[a] These deconvolution spectra of Ru are only taking into consideration metallic Ru and RuO_2 without considering hydrous ruthenium or higher oxide state species.

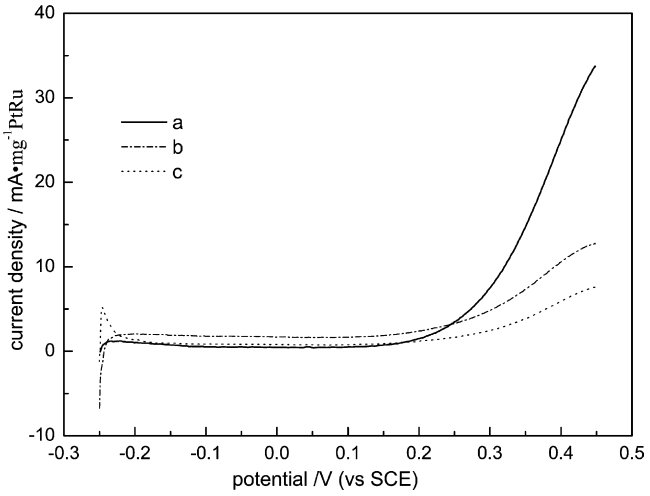

Fig. 3. Linear sweep voltammograms of methanol oxidation, 20 wt.% PtRu/C catalysts in nitrogen saturated 0.5 M CH_3OH + 0.5 M H_2SO_4 solution, room temperature, scanning rate 5 mV s^{-1}, catalyst metal loading 0.01 mg PtRu cm^{-2} before annealing (a), after annealing, 2 h at 250 °C (b) and 400 °C (c).

0.45 V. The current densities decay dramatically after annealing treatment. The higher the annealing temperature used, the lower the current density for the oxidation of methanol would proceed. This result shows that the non-annealed catalyst exhibits the best electrocatalytic activity for methanol electrooxidation probably due to temperature effects. As the temperature increases, the agglomeration takes place and the particles grow in size causing a bad dispersion of the nanoparticles and a decrease in active catalytic area. Anhydrous RuO_2, which was observed to form on annealing, does not contribute to any activity enhancement. It was the hydrous ruthenium oxide that most likely takes part in the electrooxidation activity of PtRu/C catalyst by serving as a source of active oxygen for the methanol oxidation reaction [6]. The annealing treatment was usually carried out to remove the harmful citrate stabilizer to improve the catalyst performance. However, this removal of stabilizer might limit the immobilization of the nanocrystalline particles resulting in agglomeration, size growth, and detachment from the carbon support [15]. The non-annealed electrocatalyst is better for methanol electrooxidation than that annealed at 250 °C or higher, in that the disadvantages of size growth and loss in the catalyst promoter (hydrous $RuO_2{\cdot}xH_2O$) outweigh the advantage resulting from the removal of the stabilizer.

3.2. PH effect evaluation

3.2.1. TEM and XRD analyses

In order to evaluate the stabilizing effect of citrate at different pH values, the pH of the aqueous solution was adjusted and kept at 5, 7, 9 and 13 before chemical reduction. For all the samples, no annealing treatment was carried out. Fig. 4 presents the TEM images of the prepared catalysts. By manually measuring diameters of 200 randomly selected particles with clear boundaries in TEM images, the distribution of the catalysts nanoparticles synthesized at pH 7 and 9 are obtained and shown in Fig. 4e and f, respectively. Such statistically measured mean sizes and standard deviations of synthesized catalysts at pH 5 and 11 are also listed in Table 2. The mean size of PtRu nanoparticles varies greatly with the pH values: 4.42 nm at pH 5, 2.38 nm at pH 7, 2.66 nm at pH 9, and 3.36 nm at pH 13. The TEM image shows that the well-dispersed catalyst with uniform size distribution can be obtained at pH 7 (see Fig. 4g). Thus, neither an acidic nor a basic solution, but a neutral solution is favored for stabilizing effect of the citrate. In addition, the inductively coupled plasma (ICP) of the filtrate was examined for evaluating the completeness of the reaction. The total losses of Pt and Ru were found to be below 2 wt.% within the permissible experimental error. And EDS analysis indicates the broader the area scanned, the lesser is the deviation from the designed atomic ratio of 1:1.

The XRD patterns are shown in Fig. 5. The calculated crystallite size and Ru atomic fraction in PtRu alloy are presented in Table 2. The first two peaks of Pt(1 1 1) and Pt(2 0 0) overlap each other due to the broadening effect of nanoparticles except for the catalyst prepared at pH 5. No distinct metallic ruthenium or anhydrous ruthenium oxide was detected in any of the samples. The Pt fcc structure shows certain degree of alloying with Ru, which was calculated through the peaks of fcc (2 2 0). The pattern is shown in the insert in Fig. 5. As presented in Table 2, the mean sizes basically agree with the statistically obtained data from TEM analysis. The minimum size occurs when the pH value was kept at 7 consistent with TEM results. As for alloying structure, more PtRu alloy was formed at the higher pH values. The ruthenium fraction reaches 46.75% at pH 13, almost half the catalyst bulk amount. Ruthenium was present in the form of metallic alloy with platinum and not as hydrous ruthenium oxide. It may be concluded that the alloying degree of PtRu/C catalysts can be controlled by the stabilizing pH.

3.2.2. Stabilizing pH effects

The dependence of the citrated-stabilized PtRu/C catalysts on the stabilizing pH could be discussed as follows. The stabilizing effect of citrate anion directly relates to the chemical equilibrium of citrate. The solution pH should be kept above the pK_{a3} of citric acid, namely 5.66 to ensure the deprotonation of citric acid and the functioning of citrate stabilizer. As for the catalyst prepared at pH 5, the particle growth might result from a lack of citrate anion (cit^{3-}) [16]. For other samples, in the presence of citrate anion, it is proposed that the citrate complexation of Pt(IV) would be formed to realize the stabilizing effect [14]. At the same time, the hydrolysis of $PtCl_6^{2-}$ [23] occurs in basic solution in competition with the citrate complexation reaction of Pt(IV). The hydrolyzed products become dominant in a solution with a high pH value and hence the citrate complexation of Pt(IV) may be disfavored in a high pH solution, which leads to the malfunction of citrate anion as a stabilizer. Moreover, an increase of pH value may result in the increase of the ion strength in the solution. Even the citrate complexation occurs at high pH value, the strong ion strength destabilizes the citrate-stabilized platinum hydrosol particles. The electrostatic interaction between non-occupied electrons of citrate anion and negatively charged carbon surface repulse each other [24] leading to agglomeration or the non-homogeneous distribution on carbon support. In addition, the alloying degree of PtRu/C catalysts

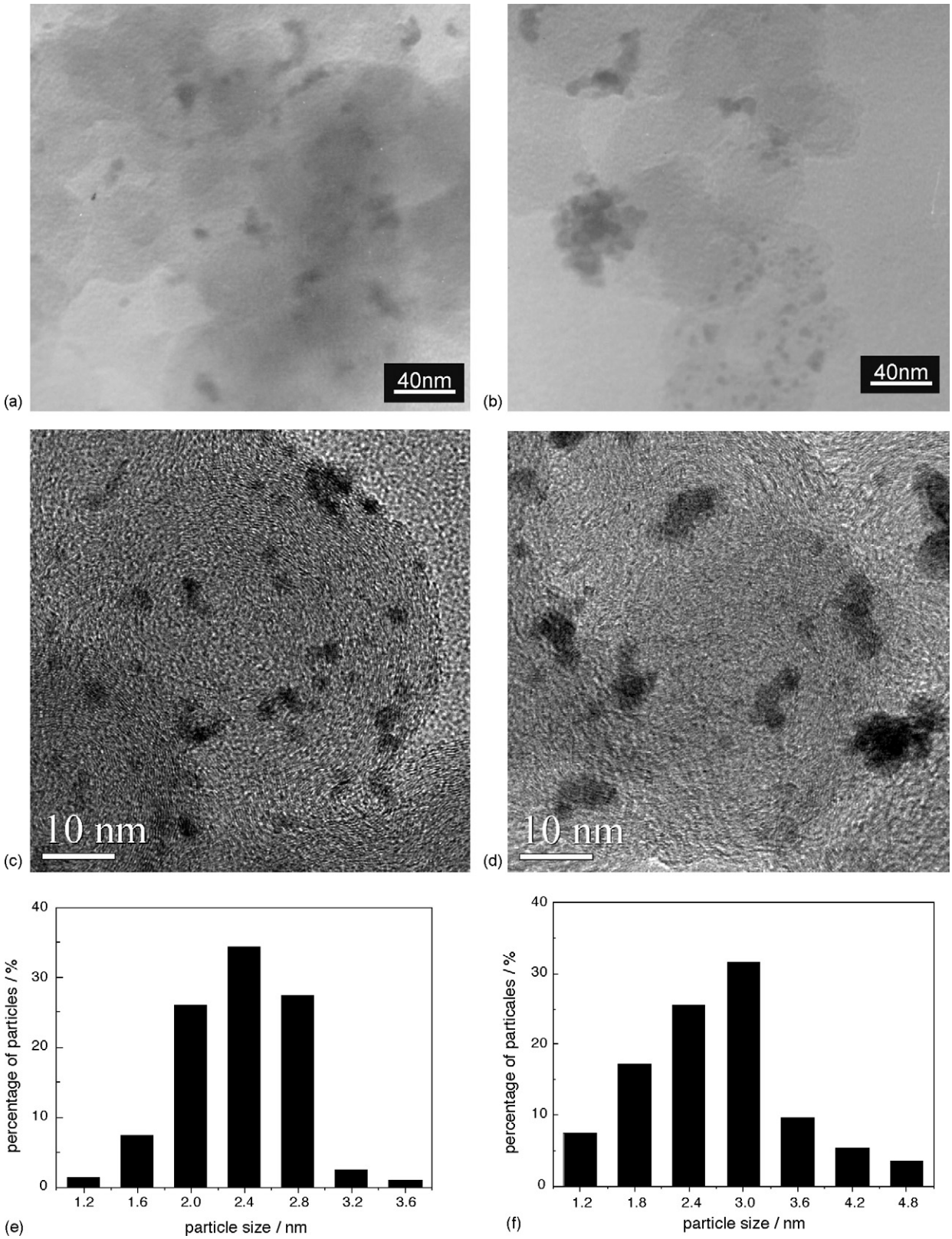

Fig. 4. LM-TEM images of citrate-stabilized 20 wt.% PtRu/C catalysts prepared at pH 5 (a) and 13 (b); the HR-TEM images of citrate-stabilized 20 wt.% PtRu/C catalysts prepared at pH 7 (c) and 9 (d); size distribution for catalysts prepared at pH 7 (e) and 9 (f); LM-TEM images of citrate-stabilized 20 wt.% PtRu/C catalysts prepared at pH 7 (g).

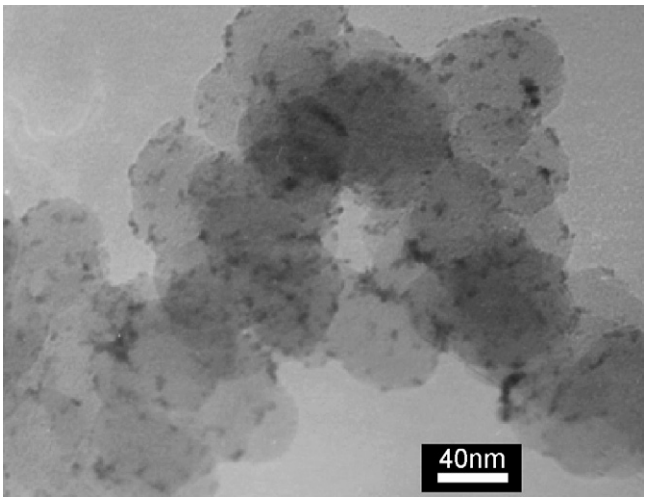

Fig. 4. (*Continued*).

Table 2
Characterization results of XRD, TEM and Electrochemical performance for citrate-stabilized 20 wt.% PtRu/C catalysts prepared at different pH values

Citrate-stablized 20 wt.% PtRu/C catalysts	$2\theta_{max}$	$B_{2\theta}$ (°)	Ru fraction (at%)[a]	Particle size (nm)		Electrochemical activities	
				XRD	TEM	Onset Potential (V)[b]	Current density at 0.45 V (mA mg^{-1} PtRu)
Varied pH values							
5	67.7	1.78	2.36	5.31	4.42 ± 2.14	–	3.5
7	68.0	3.7	14.62	2.56	2.39 ± 0.46	0.12	66.4
9	68.4	3.5	30.78	2.71	2.58 ± 0.62	0.15	40.1
11[c]	68.5	3.5	34.80	2.72	–	0.17	33.9
13	68.8	2.7	46.75	3.52	3.36 ± 1.45	0.2	13.5

[a] Ru atomic fraction in PtRu alloy according to Vegard's law.
[b] Onset potential is estimated from difference between LSV in 0.5 M H_2SO_4 and 0.5 M H_2SO_4 + 0.5 M CH_3OH; potentials are vs. SCE.
[c] Data of catalyst synthesized at pH 11.

can be controlled by the stabilizing pH due to the steric resistance among citrate complexation of Pt(IV). With less Pt(IV) complexed with citrate at high pH solution, more ruthenium precursor might quickly transfer and be reduced into the alloy lattices without steric resistance from citrate anion stabilizer.

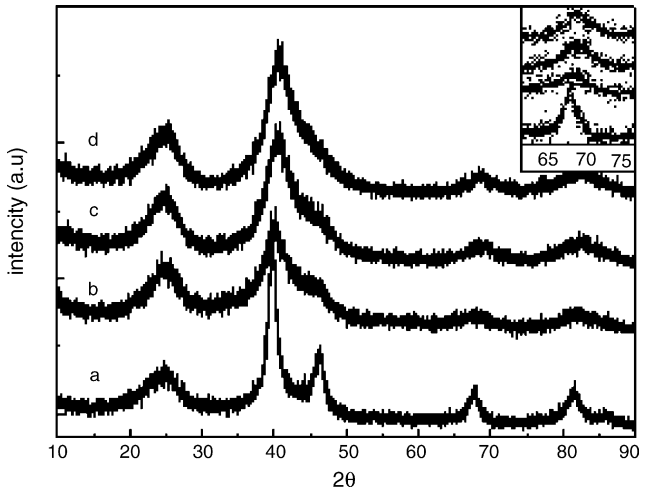

Fig. 5. XRD patterns of citrate-stabilized 20 wt.% PtRu/C catalysts prepared at pH 5 (a), 7 (b), 9 (c), and 13 (d); insert profile Pt(2 2 0).

3.2.3. Electrochemical characterization

Methanol electrooxidation on catalysts synthesized at different stabilizing pH values were tested and the results are presented in Fig. 6. The catalyst prepared at pH 5 had nearly no activity. And at the neutral condition (pH 7), catalyst showed the highest methanol oxidation current density of 66.4 mA mg^{-1} PtRu measured at 0.45 V. The current density decreased as the pH increased, 40.1 mA mg^{-1} and 13.5 mA mg^{-1} PtRu at pH 9 and 13, respectively. The onset potentials were estimated from the difference between the LSV in 0.5 M H_2SO_4 and 0.5 M H_2SO_4 + 0.5 M CH_3OH. These results are also summarized in Table 2. The lower onset potential for methanol oxidation corresponds to the higher electrocatalytic activity, indicating a better availability of active oxygen, which is required for the methanol oxidation reaction. Therefore, the catalyst synthesized at pH 7 exhibited superior electrocatalytic activity with the lowest onset potential for methanol electrooxidation.

3.3. Fuel cell performance

Based on the LSV results, the performance test on a single DMFC with citrate-stabilized 20 wt.% PtRu/C catalysts synthesized at pH 7 as anode catalysts was conducted at 65 °C and 75 °C. The results are presented in Fig. 7. The voltage was seen

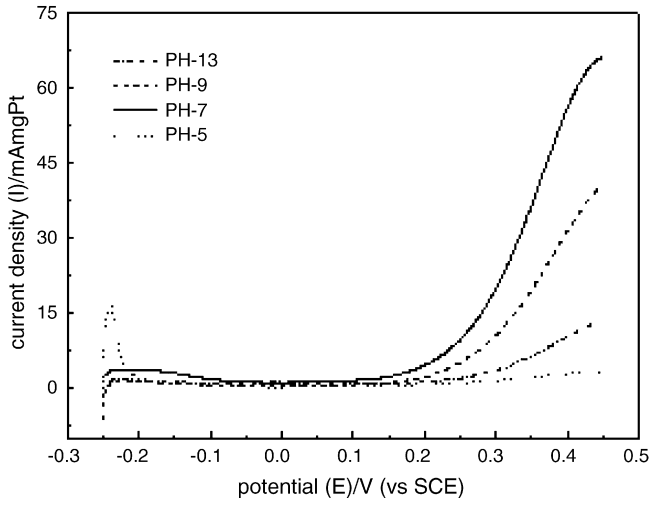

Fig. 6. Linear sweep voltammograms of methanol oxidation, 20 wt.% PtRu/C catalysts prepared at different pH, in nitrogen saturated 0.5 M CH_3OH + 0.5 M H_2SO_4 solution, room temperature, scanning rate 5 mV s^{-1}, metal loading 0.01 mg PtRu cm^{-2}.

to drop with the increasing current density. The steady-state polarization curves can be divided into the activation polarization reflecting the methanol electrooxidation at the anode and the linear ohmic polarization, mainly affected by internal resistance. There seems to be no significant mass-transfer polarization under the experimental conditions. The fuel cell when operated at 75 °C performed consistently better than at 60 °C and the difference became larger as the current density was increased. In activation polarization region, the voltage of the cell operated at 75 °C slightly exceeded when operated at 60 °C at the same current density with an open-circuit voltage (OCV) 0.021 V higher, showing a better electrocatalytic activity at a higher working temperature. Power density has also been obtained from cell potential and current density data as shown in Fig. 7. The maximum power density was 67.5 mW cm^{-2} for a DMFC performance at the current density of 240 mA cm^{-2}.

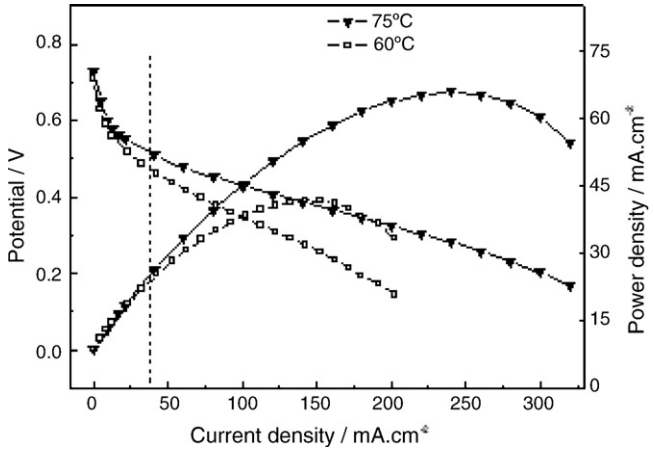

Fig. 7. DMFC performance at 60 °C and 75 °C, citrate-stabilized 20 wt.% PtRu/C catalysts prepared at pH 7, anode catalysts loading 2.73 mg PtRu cm^{-2}; cathode catalyst 60 wt.% Pt/C, metal loading 3 mg Pt cm^{-2}, 1 M methanol, flow rate 3 mL min^{-1}, air flow rate 300 sccm, zero psig.

4. Conclusion

Bimetallic PtRu/C anode catalysts were prepared by a chemical reduction method stabilized by sodium citrate in an aqueous solution. Catalyst characteristics were studied before and after annealing treatment at 250 °C and 400 °C. The non-annealed catalyst exhibits better electrocatalytic activity for methanol electrooxidation due to its small particle size and narrow size distribution, as well as enrichment in hydrous ruthenium oxide. Catalysts prepared at a stabilizing pH in the range of 5–13 were investigated for the pH effect on the catalyst activity. The results showed that a stabilizing pH 7 had the greatest effect on the electrocatalytic activity of the catalyst due to acitrate complexation stabilizing effect and the reduction in PtRu alloy. A single cell test with the prepared anode catalyst produced an output power density of 67.5 mW cm^{-2} at a current density of 240 mA cm^{-2} at 75 °C.

Acknowledgements

The work was funded by the National High Technology R&D Program of China (2003AA517070) and the Key Grant International Cooperation Project of China (2004DFB02500).

References

[1] J.B. Goodenough, R. Manoharan, A.K. Shukla, K.V. Ramesh, Chem. Mater. 1 (1989) 391–398.
[2] P.K. Babu, H.S. Kim, E. Oldfield, A. Wieckowski, J. Phys. Chem. B 107 (2003) 7595–7600.
[3] W.L. Holstein, H.D. Rosenfeld, J. Phys. Chem. B 109 (2005) 2176–2186.
[4] T. Yajima, H. Uchida, M. Watanabe, J. Phys. Chem. B 108 (2004) 2654–2659.
[5] Q. Ge, S. Desai, M. Neurock, K. Kourtakis, J. Phys. Chem. B 105 (2001) 9533–9536.
[6] J.W. Long, R.M. Stroud, K.E. Swider-Lyons, D.R. Rolison, J. Phys. Chem. B 104 (2000) 9772–9776.
[7] D.R. Rolison, P.L. Hagans, K.E. Swider, J.W. Long, Langmuir 15 (1999) 774–779.
[8] Q.Y. Lu, B. Yang, L. Zhuang, J.T. Lu, J. Phys. Chem. B 109 (2005) 8873–8879.
[9] Z.G. Chen, X.P. Qiu, B. Lu, S.C. Zhang, W.T. Zhu, L.Q. Chen, Electrochem. Commun. 7 (2005) 593–596.
[10] C. Bock, M.A. Blakely, B. MacDougall, Electrochim. Acta 50 (2005) 2401–2414.
[11] T. Iwasita, H. Hoster, A.J. Anacker, W.F. Lin, W. Vielstich, Langmuir 16 (2000) 522–529.
[12] J. Turkevich, R.S. Miner Jr., L. Babenkova, J. Phys. Chem. 90 (1986) 4765–4767.
[13] C.S. Lin, M.R. Khan, S.D. Lin, J. Colloid Interface Sci. 287 (2005) 366–369.
[14] J.W. Guo, T.S. Zhao, J. Prabhuram, C.W. Wong, Electrochim. Acta 50 (2005) 1973–1983.
[15] S.N. Pron'kin, G.A. Tsirlina, O.A. Petrii, S.Y. Vassiliev, Electrochim. Acta 46 (2001) 2343–2351.
[16] Y. Shimazaki, Y. Kobayashi, S. Yamada, T. Miwa, M. Konno, J. Colloid Interface Sci. 292 (2005) 122–126.
[17] C. Bock, C. Paquet, M. Couillard, G.A. Botton, B.R. MacDougall, J. Am. Chem. Soc. 126 (2004) 8028–8037.
[18] V. Radmilovic, H.A. Gasteiger, P.N. Ross Jr., J. Catal. 154 (1995) 98–106.

[19] E. Antolini, F. Cardellini, L. Giorgi, J. Mater. Sci. Lett. 19 (2000) 2099–2103.
[20] H.M. Villullas, F.I. Mattos-Costa, L.O.S. Bulhoes, J. Phys. Chem. B 108 (2004) 12898–12903.
[21] P.V. Samant, C.M. Rangel, M.H. Romerob, J.B. Fernandes, J.L. Figueiredo, J. Power Sources 151 (2005) 79–84.
[22] S. Rojas, F.J. Garcıa-Garcıa, S. Jaras, M.V. Martınez-Huerta, J.L.G. Fierro, M. Boutonnet, Appl. Catal. A 285 (2005) 24–35.
[23] F.X. Zhang, J.X. Chen, X. Zhang, W.L. Gao, R.C. Jin, N.J. Guan, Y.Z. Li, Langmuir 20 (2004) 9329–9334.
[24] L.Q. Jiang, L. Gao, Carbon 41 (2003) 2923–2929.